AGU ADVANCING EARTH AND SPACE SCIENCES

Water Resources Research®

RESEARCH ARTICLE
10.1029/2023WR034689

Impact of Lateral Gap on Flow Distribution, Backwater Rise, and Turbulence Generated by a Logjam

Isabella Schalko[1,2,3], **Elizabeth Follett**[4], **and Heidi Nepf**[3]

[1]Institute of Fluid Dynamics, ETH Zurich, Zurich, Switzerland, [2]Laboratory of Hydraulics, Hydrology and Glaciology (VAW), ETH Zurich, Zurich, Switzerland, [3]Department of Civil and Environmental Engineering, Massachusetts Institute of Technology, Cambridge, MA, USA, [4]Department of Civil and Environmental Engineering, University of Liverpool, Liverpool, UK

Abstract Logjams may form at natural obstructions and are also used as nature-based solutions for river restoration and natural flood management. Previous research has described backwater rise due to logjams that span the full channel cross-section and logjams with a gap between the lower edge of the logjam and the bed. Logjams that fill the channel depth, but not its width, leaving a lateral gap between the logjam and the channel bank, are also common natural formations and the focus of this study. The flow distribution between the logjam and the lateral gap, backwater rise, and wake turbulence are key factors in determining the ecologic and flood risk impact of a logjam. Specifically, relative to a channel-spanning logjam, the introduction of a lateral gap can reduce backwater rise and increase the potential for trapping particles, such as nutrients or microplastics, within the wake region, but may also promote erosion in the gap. The choice of logjam and gap widths can be used to maximize flow and habitat diversity in rivers, while reducing erosion risk. We present experimental results demonstrating that the flow distribution between the logjam and the lateral gap can be predicted by assuming equal resistance through the logjam and gap sections. Further, we show that backwater rise can be determined from the predicted discharge through the logjam using a momentum balance developed for channel-spanning logjams. Finally, turbulence generated within the jam was observed directly downstream of the logjam, and, for the densities considered, increased with jam density.

Key Points:

- Compared to channel-spanning logjams, a lateral gap reduces backwater rise, but increases local shear stress and erosion potential
- Flow distribution between logjam and gap can be predicted from total discharge, logjam resistance, and ratio of logjam to gap width
- Log-scale turbulence generated by the logjam persists in the wake for approximately 20 log diameters downstream of logjam

Supporting Information:

Supporting Information may be found in the online version of this article.

Correspondence to:

I. Schalko,
ischalko@ethz.ch

Citation:

Schalko, I., Follett, E., & Nepf, H. (2023). Impact of lateral gap on flow distribution, backwater rise, and turbulence generated by a logjam. *Water Resources Research*, *59*, e2023WR034689. https://doi.org/10.1029/2023WR034689

Received 16 FEB 2023
Accepted 19 SEP 2023

Author Contributions:

Conceptualization: Isabella Schalko
Formal analysis: Isabella Schalko, Elizabeth Follett, Heidi Nepf
Funding acquisition: Isabella Schalko
Methodology: Isabella Schalko
Project Administration: Isabella Schalko
Supervision: Heidi Nepf
Validation: Elizabeth Follett, Heidi Nepf
Visualization: Isabella Schalko, Elizabeth Follett
Writing – original draft: Isabella Schalko

1. Introduction

Wood plays an essential role in a river ecosystem, as it can create heterogeneous flow conditions and morphological structures that provide habitat for fish (Gippel, 1995; Keller & Swanson, 1979; Wohl et al., 2019). Wood transported in rivers may form a logjam in shallow water areas, at obstructions (e.g., gorges or bridges), or at a key log (Abbe & Montgomery, 2003; Davidson et al., 2015; Manners & Doyle, 2008; Nakamura & Swanson, 1994; Wallerstein et al., 1996). Depending on the ratio of channel width to log length, logjams may be channel-spanning or may only partially span the channel, with a gap between the jam and one of the channel banks (Figure 1, from herein defined as partial-spanning logjam). Livers and Wohl (2021) analyzed 183 logjams, including both channel- and partial-spanning logjams, in the Colorado Front Range and observed that partial-spanning logjams result in a significantly smaller volume of particulate organic matter stored in both backwater pools and in logjams, as well as smaller backwater pool volume.

Ecologically beneficial wakes may form downstream of logjams (similar to those behind boulders or patches of vegetation), and pools of slower water may form upstream, in which nutrients and organic matter can deposit (Beckman & Wohl, 2014; Bilby, 1981; Faustini & Jones, 2003; Skalak & Pizzuto, 2010). Logjams also increase vertical connectivity and residence time of hyporheic exchange flow (Doughty et al., 2020; Sawyer et al., 2011) and provide habitat for fish and small animals (Roni et al., 2015; Wohl et al., 2016). Tullos and Walter (2015) studied the behavior of juvenile coho salmon close to logjams and found that partial-spanning logjams can establish two types of fish habitat: regions of low velocity in the wake and upstream pool, providing shelter, and regions of increased velocity adjacent to the logjam, with higher drift encounter rates for energy gain. However, knowledge is missing to describe the extent of the two flow regions for different logjam widths.

Depending on the logjam size and the flow conditions, the resulting backwater rise (increase in upstream water depth) may lead to flooding of the surrounding area (Comiti et al., 2016; Lucía et al., 2015; Schmocker & Weitbrecht, 2013). Backwater rise due to channel-spanning logjams as well as channel-spanning logjams with a vertical gap between the channel bottom and the logjam have been described with analytical and empirical

Writing – review & editing: Isabella Schalko, Elizabeth Follett, Heidi Nepf

models (Follett et al., 2020, 2021; Schalko et al., 2018, 2019a). However, a research gap remains regarding the backwater rise due to logjams that only partially span the channel width.

Channel-spanning logjams have been shown to induce scour at the channel bed, with the degree of scour governed by wood volume and grain size characteristics (Schalko et al., 2019b). On the other hand, placement of individual wood pieces and partial-spanning logjams have been used as a tool to control erosion at the channel banks (Pagliara & Kurdistani, 2017). While the placement of individual logs near an erodible bank has been shown to increase erosion rates, the opposite was observed for logs positioned in series, as wake interference effectively reduced near-bank velocity (Zhang et al., 2020a, 2020b; Zhang & Rutherfurd, 2020).

As the recognition of ecosystem services provided by wood in rivers has broadened the perception of wood beyond simply a flood and navigation hazard (Gurnell et al., 2002; Piégay et al., 2005; Roni et al., 2015), the number of river restoration projects including wood has increased within the past decades (Roni et al., 2015). Engineered logjams (ELJ) are a common measure used in river restoration and nature-based solutions for natural flood management. Compared to natural logjams, ELJs are fixed in place and tend to have more uniform logjam characteristics (e.g., uniform wood spacing). Both natural logjams and ELJs can be described as groyne-like wooden structures used to alter the flow (Brooks, 2013). In contrast to groynes (Weitbrecht et al., 2008), ELJs are commonly emergent with a wide range of porosities and widths (Roni et al., 2015). For example, in Switzerland, ELJs are placed perpendicular to the flow direction, extending over a partial span of the channel to promote the creation of deep pools and provide cover habitat for fish (Neuhaus & Mende, 2021). While design guidelines for ELJs exist (Bureau of Reclamation & U.S. Army Engineer Research and Development Center (USBR & ERDC), 2016), they are primarily practice-based due to the lack of analytical tools to predict the local flow and turbulent structures for different ELJ layouts. To improve the design of ELJs and the analysis of existing natural logjams, this study provided new tools to answer the following research questions: (a) How can the flow distribution between the logjam and the adjacent open flow section be quantified?, (b) Can existing equations that have been derived for channel-spanning logjams be applied to predict backwater rise due to partial-spanning logjams?, and (c) How can the turbulence levels in the logjam wake be estimated? The new quantitative tools were used to explore optimal jam width with respect to backwater rise (flooding potential), erosion, and generation of flow heterogeneity to improve habitat.

We conducted physical model tests to study the hydrodynamic response to logjams on a solid bed. The logjams spanned different fractions of the channel width and had different porosities (solid volume fraction). The water depth, time-mean velocity, and turbulent kinetic energy generated by the partial-spanning jams (PSJ) were compared to channel-spanning jams (CSJ). The experiments were conducted for different flow velocities, modeling low and high flows. Our study demonstrated that the distribution of flow between the logjam and the lateral gap can be determined based on the assumption that the jam and lateral gap sections act as parallel resistors with equal momentum loss. Using the predicted discharge through the logjam, the backwater rise was predicted using the analytical model presented in Follett et al. (2020). Finally, we adapted the turbulence model by Tanino and Nepf (2008) for rigid arrays to predict turbulence levels directly downstream of the logjam. The implications for local flooding, the potential for lateral scour, and flow heterogeneity are discussed.

2. Background and Theory

Because we focused on a logjam with a lateral gap between the jam and the flume wall (Figure 2), we began by describing the distribution of flow between the jam and the adjacent gap, and then used the flow properties through the jam to predict the backwater rise. The partitioning of flow between the gap and the jam can be determined by assuming that these flow sections act as resistors in parallel responding to the same hydrostatic pressure gradient.

A momentum balance was considered between cross-sections 2 and 3 in Figure 2. At these cross-sections, the water depth at the jam (subscript j) and the gap (subscript g) were assumed to be equal (i.e., $h_{2,j} \approx h_{2,g}$ and $h_{3,j} \approx h_{3,g}$), and this was confirmed in the flume experiments considered here (see Results section). Specifically, the lateral variation in the water depths h_2 and h_3 was 7.5 ± 1.8% (mean ± standard error). Further, using measured velocity, we found that the vertical acceleration $u\frac{dw}{dx}$ with u longitudinal velocity, w vertical velocity, and x longitudinal direction, was small compared to gravity g, so that it is reasonable to assume hydrostatic pressure at positions 2 and 3 (see Supporting Information S1). Thus, the pressure drop driving flow through the gap and the jam is the same.

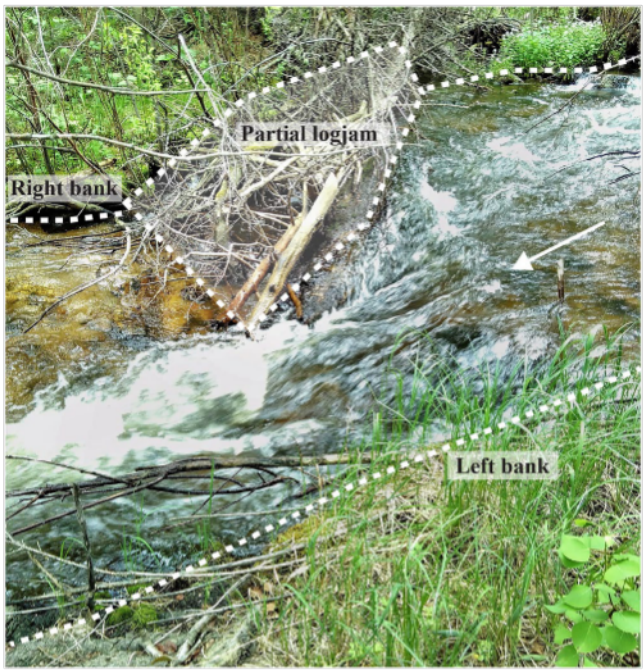

Figure 1. Logjam spanning partial width of Beaver Creek; flow direction from right to left shown by white arrow (Colorado, USA; photo: I. Schalko). White dashed curves delineate the banks and the contours of the logjam. Regions up- and downstream of jam may serve as shelter for fish, while region adjacent to jam can provide higher drift encounter rates for energy gain (Tullos & Walter, 2015).

Follett et al. (2020) detailed the momentum balance through a CSJ, showing that the change in momentum was negligible compared to the hydrostatic pressure gradient, so that the discharge through a jam of width B_j can be defined by

$$0.5\rho g B_j\left(h_2^2 - h_3^2\right) - 0.5\rho B_j L_j C_d a h_3 u_{3,j}^2 \frac{1}{(1-\phi)} = 0 \quad (1a)$$

Similarly, we can define a resistance coefficient for the gap, C_g, that describes the discharge through the gap of width B_g that is possible for a given pressure gradient

$$0.5\rho g B_g\left(h_2^2 - h_3^2\right) - 0.5\rho B_g C_g h_3 u_{3,g}^2 = 0 \quad (1b)$$

The first term in Equations 1a and 1b is the net hydrostatic pressure force, with ρ the water density, and g the gravitational acceleration. The second term in Equation 1a is the drag within the jam, with L_j the jam length, C_d the drag coefficient, a the jam-average frontal area per logjam volume, defined as $a = (4\,\phi)/(\pi\,d)$ with ϕ the solid volume fraction, and d the log diameter. The second term in Equation 1b is the flow resistance of the gap.

Because the first term in Equations 1a and 1b is the same, we can combine these equations into

$$0.5\rho B_j L_j C_d a h_3 u_{3,j}^2 \frac{1}{(1-\phi)} = 0.5\rho B_g C_g h_3 u_{3,g}^2 \quad (2)$$

with $u_{3,j}$ the laterally- and time-averaged longitudinal velocity in the jam and $u_{3,g}$ the laterally- and time-averaged longitudinal velocity in the gap. C_g is the empirically-derived gap resistance coefficient (see Results section), which is a function of logjam width to gap width ratio B_j/B_g. Specifically, $C_g = \alpha_g\,(B_j/B_g)$ with constant α_g. Equation 2 can be rearranged to solve for the fraction of channel discharge going through the logjam Q_j/Q:

$$\frac{Q_j}{Q} = \frac{1}{1 + \left(\frac{B}{B_j} - 1\right)\sqrt{\frac{L_j C_d a}{\alpha_g(1-\phi)}}} \quad (3)$$

In which B is the total channel width and Q is the total channel discharge.

The gap resistance coefficient C_g was found by fitting the measured values, indicated with subscript m, of $Q_{j,m}/Q_m$ to Equation 3 (see Results section). The measured discharge through the logjam $Q_{j,m}$ was obtained by averaging lateral profiles directly up- and downstream of the logjam, with $Q_{j,m} = (u_{2,j}\,h_2\,B_j + u_{3,j}\,h_3\,B_j)/2$ (Figure 2a). The total discharge through the section Q is the sum of discharge through the logjam Q_j and discharge through the gap Q_g.

Once the discharge through the jam Q_j was determined, the upstream water depth h_1 (with $h_1 \cong h_2$ within measurement error) was predicted from the approach in Follett et al. (2020) that combines energy and momentum constraints.

$$h_1 = \sqrt{h_3^2 + \frac{C_A {q_j}^2}{g h_3}} \quad (4)$$

The jam resistance is characterized by dimensionless $C_A = L_j C_d a/(1-\phi)^3$. For PSJ, the unit discharge was defined as $q_j = Q_j/B_j$ based on Equation 3. The water depth at the downstream edge of the logjam h_3 is the maximum value of either the downstream water depth h_4 (equal to the water depth prior to jam addition, which we call the reference water depth h assuming uniform flow conditions) or the water depth derived based on the assumption of minimum energy loss through the jam according to Follett et al. (2020).

$$h_3 = \max\left(h_4, \sqrt[3]{\frac{C_A {q_j}^2}{2g}}\right) \quad (5)$$

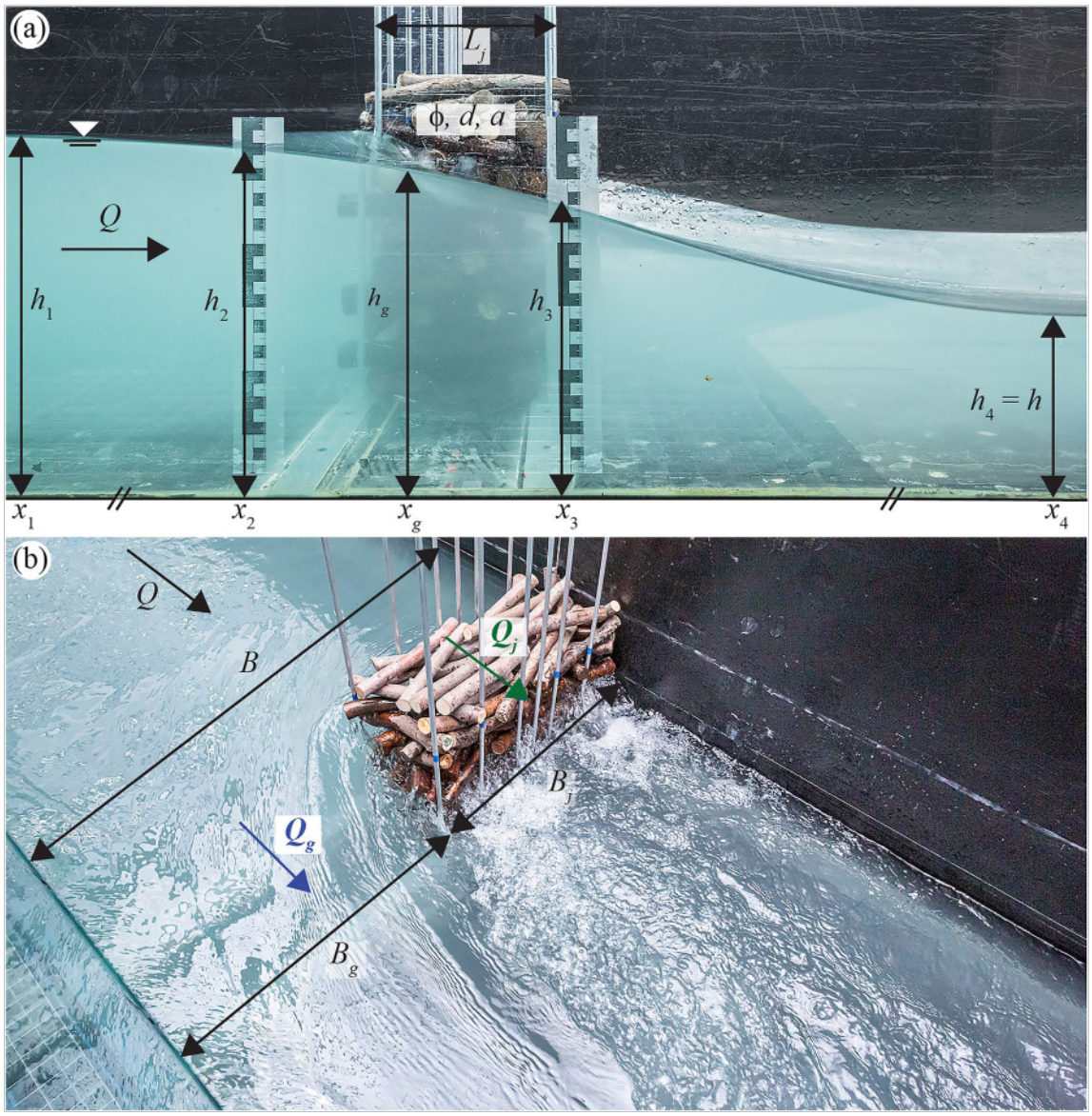

Figure 2. (a) Side and (b) top view of test setup with partial-spanning logjam with Q = total discharge, L_j = logjam length in streamwise direction, ϕ = jam solid volume fraction, d = log diameter, and a = frontal area per logjam volume. Cross-sections correspond to longitudinal distances x_1, x_2, x_g, x_3, x_4 with water depths h_1, h_2, h_g, h_3, h_4 measured relative to the channel bed. B = channel width, B_g = gap width, Q_g = discharge through gap, B_j = jam width, Q_j = discharge through jam. Note that $x = 0$ was defined at the center of the jam, corresponding to $x = x_g$. h_2 and h_3 were measured 8 cm up- and downstream of the jam, respectively, but may appear distorted due to parallax. h_1 and h_4 were measured 1 m up- and downstream of the logjam, respectively.

In cases for which h_3 was equal to h_4, Equation 4 was applied to determine h_1. When h_3 was greater than h_4, falling water was observed on the downstream edge of the jam (e.g., Figure 2). That is, water exited the jam at an elevation greater than the local flow depth. For conditions with falling water ($h_3 > h_4$ with $h_{3,\min} = \sqrt[3]{\frac{C_A q_j^2}{2g}}$), Equations 4 and 5 combine to (Supporting Information S1 for derivation)

$$h_1 = \sqrt{3}\, h_{3,\min} \tag{6}$$

The drag coefficient for the logs within the jam, C_d, was estimated for channel-spanning logjams (Schalko et al., 2018) using measured values of water depth and discharge in Equations 4 and 5. The mean drag coefficient across all tested jams was $C_{d,m} = 1.2 \pm 0.6$ (mean $\pm$ standard deviation, see Figure S1 in Supporting Information S1), which was comparable to $C_d = 0.9$ to 1.4 from previous studies on individual logs (Gippel, 1995; Shields & Alonso, 2012).

Note that the data spread was smaller for jams closer to prototype scale (geometric model scale factor $\lambda = 6$ used in Schalko et al. (2018), circles in Figure S1 in Supporting Information S1), but otherwise had no clear trend with pore scale Reynolds number $Re_s = U\,s/(\nu\,(1-\phi))$, with U = cross-sectional average flow velocity, ν = kinematic viscosity, and s = mean surface-to-surface distance between the logs defined as $s = (^{d}/_{a})^{1/2} - d$ (see Figure S9 in Supporting Information S1 for a graphical illustration). For the subsequent analysis, $C_d = 1.2 \pm 0.6$ was assumed.

3. Materials and Methods

Flume experiments were conducted at the Laboratory of Hydraulics, Hydrology and Glaciology (VAW) of ETH Zurich in a 10.7 m long, 1.0 m wide, and 0.8 m deep tilting channel with a fixed bed. The 2.0 m long intake was equipped with a flow straightener to condition the flow. The test setup and notation are illustrated in Figure 2. The channel had a fixed bed and side walls made of glass and PVC. Flow discharge Q was measured in the supply pipes with an electromagnetic flow meter (±1%) and regulated with a valve. The cross-sectional average flow velocity was defined as $U = Q/(B\,h)$, with B = channel width and h = reference water depth prior to placing the logjam in the channel. The initial or reference flow conditions, representing uniform and steady flow without a logjam present, were controlled by adjusting the channel slope S, Q, and a downstream flap gate. The reference flow Froude number $F = U/(g\,h)^{0.5}$, with g = gravitational acceleration ranged between F = 0.1 and 0.6 (Table 1). Note that supercritical flow (F > 1) was observed in the gap for some tests (tests 6, 8, 9, 13, 16).

The logjam was placed 4 m downstream of the channel inlet and constructed from natural wooden logs with diameter $d = 0.027 \pm 0.003$ m (mean ± standard deviation) and length $L = 0.25 \pm 0.01$ m. The logs were placed between two rack rows (Figures 2a and 2b) with a logjam length of $L_j = 0.20$ m (measured in streamwise direction), logjam height of $H_j = 0.34$–0.49 m, and different logjam widths, $B_j = 1.00$, 0.90, 0.75, 0.50, and 0.25 m, measured in the cross-stream direction. The logjams had solid volume fractions of $\phi = 0.40$, $\phi = 0.50$, and $\phi = 0.21$, with $\phi = V_s/V_t$ defined as the ratio of solid wood volume V_s (sum of log volume in jam) to total jam volume V_t ($B_j \times L_j \times H_j$). These corresponded to spatially-averaged frontal area per jam volume $a = (4\,\phi)/(\pi\,d)$ of $a = 18.9 \pm 0.7$ m^{-1}, $a = 23.7 \pm 0.4$ m^{-1}, and $a = 9.8 \pm 0.5$ m^{-1}, respectively. The solid volume fraction and frontal area per logjam volume are related by the log diameter d. The dimensionless structural parameter $C_A = L_j\,C_d\,a/(1-\phi)^3$ was determined according to Follett et al. (2020) with $C_A = 21 \pm 3$ (mean ± standard deviation; for $\phi = 0.40$); $C_A = 44 \pm 3$ ($\phi = 0.50$), and $C_A = 5 \pm 1$ ($\phi = 0.21$).

The water depth was measured along longitudinal and lateral profiles using an Ultrasonic Distance Sensor (UDS; ±0.3 mm) with an 8 cm measurement cone positioned on an automated traverse system. The velocity (streamwise u, lateral v, and vertical w) was measured along longitudinal, lateral, and vertical profiles up- and downstream of the logjam using Acoustic Doppler Velocimetry (Nortek Vectrino). A side-looking probe used a 200 Hz sampling rate for 240 s, over which duration the mean and turbulent flow statistics reached convergence. The velocity records were despiked and filtered according to Goring and Nikora (2002). Each velocity record was decomposed into time-mean ($\overline{u}, \overline{v}, \overline{w}$) and fluctuating ($u'$, v', w') components using a MATLAB script. The turbulent kinetic energy was

$$k_t = 0.5\left(\overline{u'^2} + \overline{v'^2} + \overline{w'^2}\right) \tag{7}$$

The noise level of the ADV probe was evaluated to be 0.10 cm^2/s^2, which is below the measured turbulence levels in this study.

Longitudinal profiles of water depth, velocity, and turbulent kinetic energy were taken at the center of the jam and the center of the gap. To simplify measurement along a transect, the velocity measurements were conducted at a constant distance above the channel bed ($z = 0.1$ m), which corresponded to mid-depth for reference (without jam) flow condition, and it generally provided a good approximation for depth-averaged velocity. Vertical velocity profiles at selected locations are provided in Supporting Information S1 (Figures S6–S8). In addition, lateral profiles of velocity and turbulent kinetic energy at $z/h = 0.5$ were measured 8 cm upstream, as well as 8 cm and 2.4 m downstream of the logjam to obtain laterally-averaged values of u and k_t in the vicinity of the logjams (see Figures S4 and S5 in Supporting Information S1).

To start (tests 1–3), channel-spanning logjams were investigated with $\phi = 0.41$, 0.49, 0.20. Next, experiments were conducted for $\phi = 0.40$ with progressively smaller logjam width $B_{j,rel} = B_j/B$ with $B_{j,rel} = 0.90$ (tests 4–6),

Water Resources Research

10.1029/2023WR034689

Table 1
Test Program With Reference Water Depth h = 0.20 m, Jam Length L_j = 0.20 m, and Average Log Diameter d = 0.027 ± 0.003 m (Mean ± Standard Deviation)

Test	Reference flow velocity	Discharge	Reference froude number	Relative logjam width	Logjam height	Solid wood volume	Total jam volume	Solid volume fraction
#	U [m/s]	Q [m^3/s]	F [-]	$B_{j,rel}$ [-]	H_j [m]	V_s [m^3]	V_t [m^3]	ϕ [−]
1	0.10	0.020	0.07	1.00	0.40	0.032	0.080	0.41
2	0.10	0.020	0.07	1.00	0.40	0.040	0.080	0.49
3	0.10	0.020	0.07	1.00	0.30	0.012	0.060	0.20
4	0.10	0.020	0.07	0.90	0.49	0.035	0.090	0.40
5	0.30	0.060	0.21	0.90	0.49	0.035	0.090	
6	0.50	0.100	0.36	0.90	0.49	0.035	0.090	
7	0.10	0.020	0.07	0.75	0.39	0.023	0.058	
8	0.50	0.100	0.36	0.75	0.38	0.023	0.057	
9	0.80	0.159	0.57	0.75	0.38	0.023	0.058	
10	0.10	0.020	0.07	0.50	0.39	0.015	0.039	
11	0.30	0.060	0.21	0.50	0.40	0.015	0.039	
12	0.50	0.100	0.36	0.50	0.39	0.015	0.039	
13	0.80	0.159	0.57	0.50	0.39	0.015	0.039	
14	0.10	0.020	0.07	0.25	0.39	0.008	0.019	
15[a]	0.50	0.100	0.36	0.25	0.39	0.008	0.019	
16	0.80	0.159	0.57	0.25	0.34	0.008	0.017	
17	0.10	0.020	0.07	0.50	0.40	0.020	0.039	0.51
18	0.30	0.060	0.21	0.50	0.40	0.020	0.039	
19	0.50	0.100	0.36	0.50	0.40	0.020	0.039	
20	0.30	0.060	0.21	0.50	0.40	0.008	0.039	0.21
UC	*0.01*	*0.01*	*0.01*	*0.04*	*0.025*	*0.05*		*0.10*

Note. Typical fractional uncertainties (UC) are indicated in the last row for each variable in italic, based on measurement uncertainty in individual flow characteristics and repetitive measurements of jam characteristics. Test 15 was conducted twice to investigate reproducibility. The repeated test has been used for the subsequent analysis.

[a]Reproducibility test.

$B_{j,rel} = 0.75$ (tests 7–9), $B_{j,rel} = 0.50$ (tests 10–13), and $B_{j,rel} = 0.25$ (tests 14–16). For tests 17–20, the solid volume fraction of the logjam was varied; $\phi = 0.51$ (tests 17–19) and $\phi = 0.20$ (test 20). For tests 4–19, different reference flow velocities $U = 0.10$–0.80 m/s were tested to model both baseflow conditions and high flows. The test program is summarized in Table 1. Test 15 was conducted twice to study the reproducibility, with average deviations of 0.8% in water depth, 24% in flow velocity, and 20% in turbulent kinetic energy (see Figure S2 in Supporting Information S1).

4. Results

4.1. Flow and Wake Characteristics

Longitudinal profiles of water depth, velocity, and turbulent kinetic energy were measured at the lateral centers of the jam (subscript j) and of the gap (subscript g) and normalized based on the reference water depth h and channel-average velocity U without jam placement (Figure 3). The streamwise center of the jam was defined as $x = 0$.

As presented in previous studies, CSJ generate an increase in upstream water depth and associated decrease in upstream velocity (Follett et al., 2020; Schalko et al., 2018). If the jam presented in Figure 3 were a channel-spanning logjam, it would produce a backwater rise $h_j/h = 1.9$ (based on Equation 4; additional longitudinal profiles can be found in the Supporting Information S1 in Figure S3). The backwater rise was significantly reduced from this value by the introduction of a gap between the jam and one side-wall, and decreased from $h_j/h = 1.8$ to 1.1 as the gap width increased (Figure 3a, tests 6, 8, 12, 15 in Table 1 and see decreasing jam width B_j in legend), and more flow was diverted to the open gap section (Figure 3d). The backwater rise was essentially the same in the jam and gap section, with a maximum deviation of 10% between h_j and h_g (Figures 3a and 3b). This supports the assumption made in the theory section that the lateral variation in water depth approaching the jam and far downstream of the jam is negligible. However, a significant lateral variation was observed directly downstream of the jam for the smallest gap width, which induced the highest gap velocity (darkest gray symbols in Figures 3a–3d). Directly downstream of the jam, the velocity in the jam wake was reduced compared to the condition without jam placement, with $u_j/U < 1$, while the velocity in the gap was accelerated up to $u_g/U = 3.3$ for $B_j = 0.90$ m (Figures 3c and 3d). Further, the normalized turbulent kinetic energy $k_{t,j}/U^2$ increased directly behind the logjam (Figure 3e). In the gap section, turbulence elevation was not as pronounced as in the jam section (Figure 3f).

Backwater rise increased with increasing channel-average velocity U (Figure 4; tests 10, 12, 13 in Table 1), due to the associated increase in jam drag, which resulted in a decrease in velocities u_j and u_g upstream of the logjam (Figures 4a–4d). For $B_j/B = 0.5$, the effect of U on the backwater rise was not as pronounced as the jam width B_j (Figure 3a vs. Figure 4a). However, a stronger response to U would be expected for the smallest gap ($B_j/B = 0.90$). The time-mean velocity and turbulent kinetic energy tended to collapse when normalized by channel velocity, confirming that they both scale with U. The peak turbulence was observed directly downstream of the jam (Figure 4e). The highest values of $k_{t,g}/U^2$ in the gap were observed for the case with lowest U (Figure 4f, gray squares). For this case, the ADV sampling timescale at 200 Hz ($t_s = 0.005$ s) was smaller than the Kolmogorov timescale ($t_\eta = 0.014$ s; Pope, 2000), so the measurement was able to capture close to the full turbulence spectrum.

The solid volume fraction of logjams in rivers can have a range of $\phi = 0.2$ to 0.5 (Livers et al., 2020), which was the range tested in this study. The water depth and velocity for different ϕ agreed on average within 10% (Figures 5a–5d; tests 11, 18, 20 in Table 1), but a denser accumulation (higher ϕ) produced higher turbulent kinetic energy directly downstream of the jam (Figure 5e). Specifically, the peak turbulence intensity was 2.9 times higher for $\phi = 0.5$ compared to $\phi = 0.2$. However, if solid volume fraction increased further, eventually flow through and turbulence generated within the jam would likely diminish.

4.2. Flow Distribution and Backwater Rise

First, the gap resistance coefficient $C_g = \alpha_g B_j/B_g$ was determined by fitting the measured values of $Q_{j,m}/Q$ to Equation 3, resulting in $\alpha_g = 1.06 \pm 0.14$ ($\pm$ standard error; with 95% confidence interval (0.75, 1.37); coefficient of determination $R^2 = 0.89$). Using the fitted gap resistance coefficient $C_g = 1.1$ (± 0.1) B_j/B_g, the discharge through the logjam was estimated by applying Equation 3, which assumes equal flow resistance in the jam and

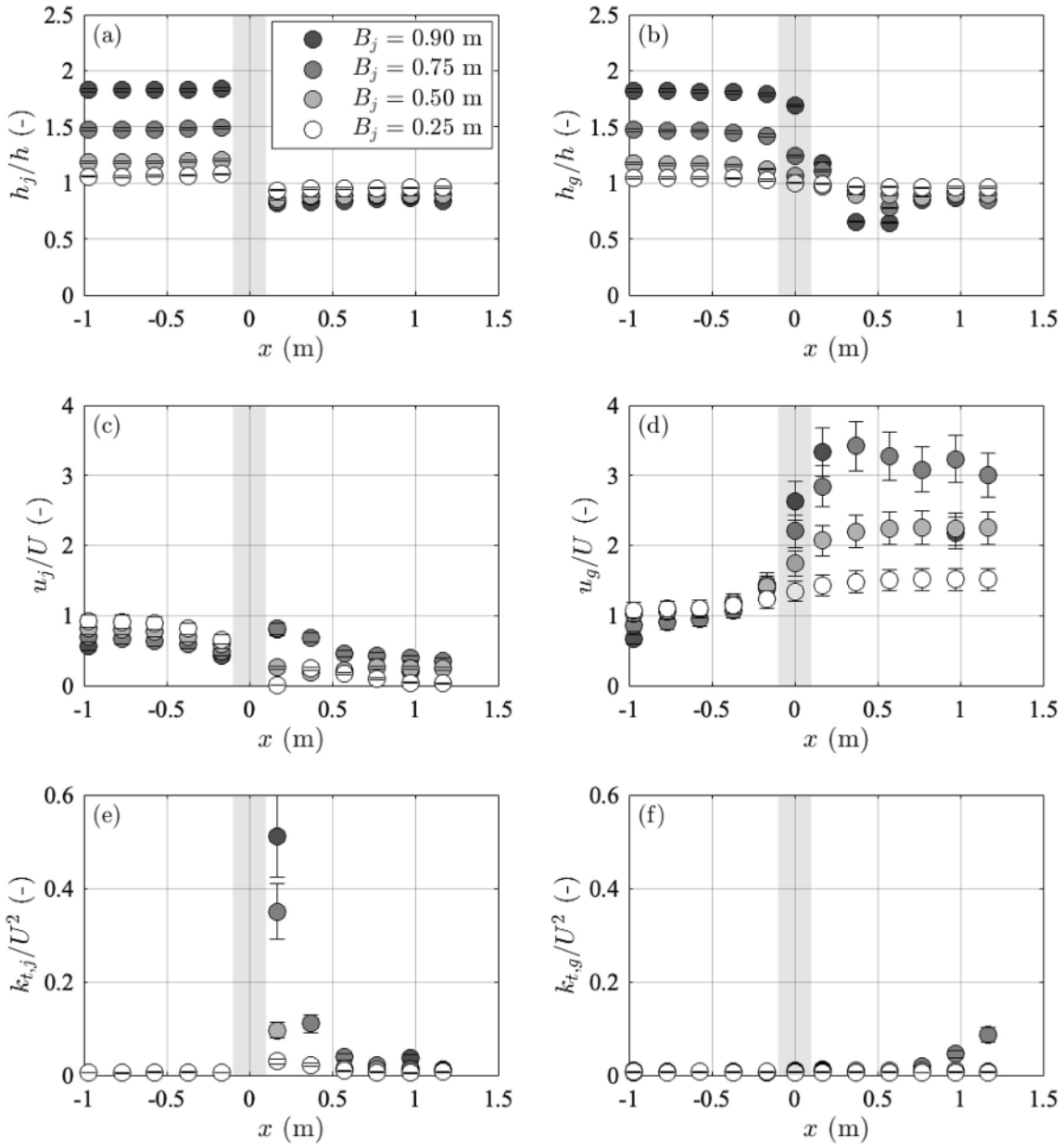

Figure 3. Longitudinal profiles of water depth normalized by the reference water depth h (a, b), and time-mean velocity (c, d) and turbulent kinetic energy (e, f) normalized by the channel-average reference velocity U. Left-hand column shows transects in line with the jam center (a, c, e), denoted by subscript "j." Right-hand column shows transects in line with the gap (b, d, f), denoted by subscript "g." Symbol shape indicates logjam width $B_j = 0.90$, 0.75, 0.50, 025 m. In all cases $U = 0.50$ m/s, $\phi = 0.40$ (tests 6, 8, 12, 15 in Table 1).

gap cross-sections. Figure 6a illustrates how the fraction of discharge passing through the logjam increased with increasing B_j and decreasing ϕ (see color bar in Figure 6a). The circles correspond to measured values of $Q_{j,m}/Q$, and the corresponding colored curves in Figure 6a show the respective solutions of Equation 3 for different ϕ (see color bar in Figure 6a). Note that variation in ϕ corresponded to different jam characteristics, including different a and C_A values.

Using Q_j determined from Equation 3, the upstream water depth h_1 (with $h_1 \cong h_2$ within measurement error) was predicted using Equations 4–6. The linear fit between measured h_1 (at the logjam section) and predicted $h_1 \cong h_2$ of the PSJ (tests 4–20, Table 1) had a slope 0.93 (with 95% confidence interval (0.88, 0.99)) found from linear regression in Matlab (Figure 6b, circles). CSJ from Schalko et al. (2018) and this study (tests 1–3, Table 1) are plotted for comparison in Figure 6b (CSJ-I plotted as squares and CSJ-II as diamonds).

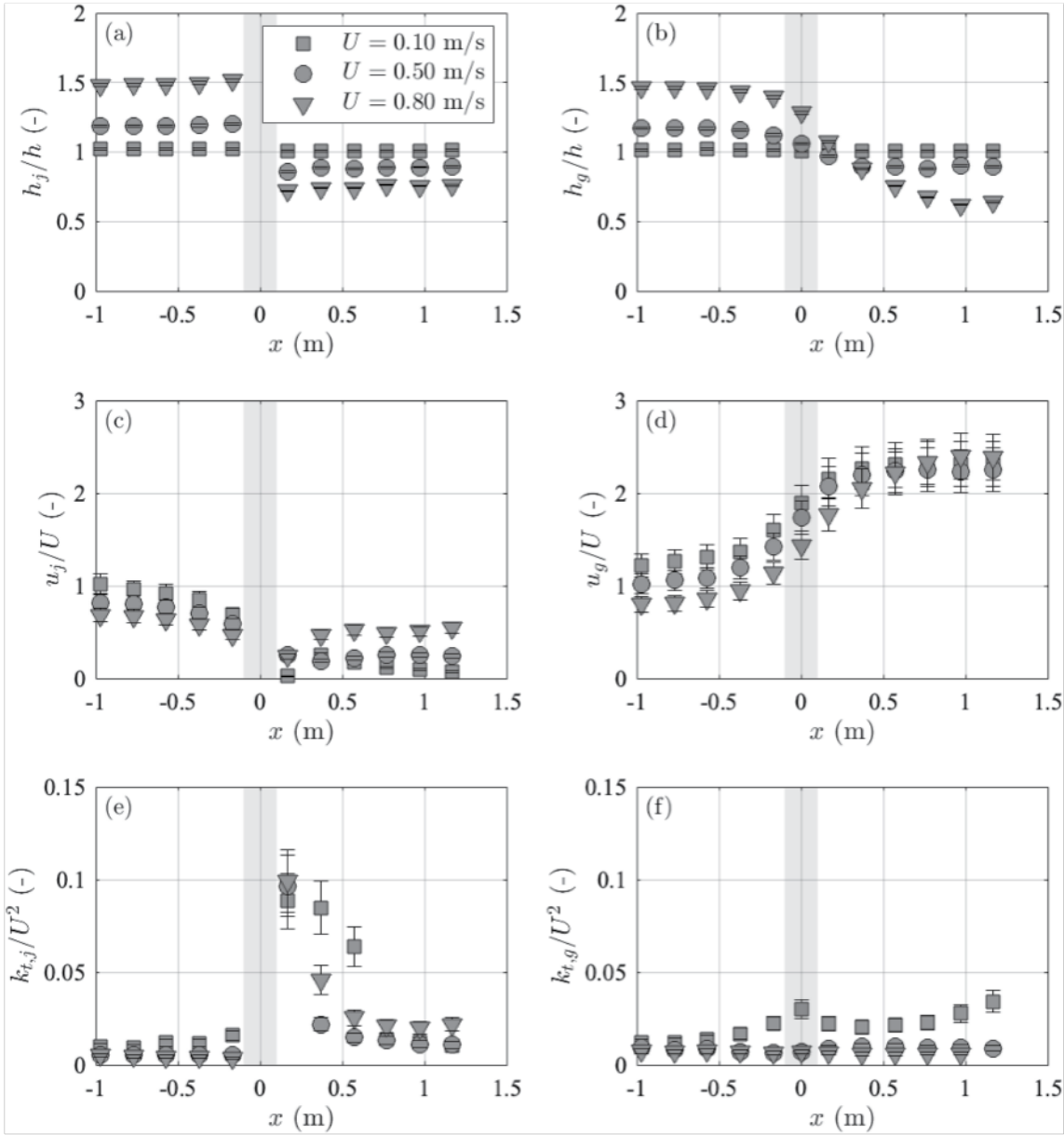

Figure 4. Longitudinal profiles of normalized water depth, time-mean velocity, and turbulent kinetic energy along the jam center (a, c, e) and gap center (b, d, f) for different reference velocities $U = 0.10$, 0.50, 0.80 m/s and for $B_j = 0.50$ m, $\phi = 0.40$ (tests 10, 12, 13 in Table 1).

An error propagation analysis was conducted for Equations 3 and 4–6 (Martin & Pohl, 2015). The average relative error of Equation 3 was 20% and for Equations 4–6 16%. These values are plotted as shaded areas in Figure 7 to highlight the associated uncertainties. Additional information on the error propagation is provided in the Supporting Information S1 (Table S1).

5. Discussion

5.1. Effect of Logjam Characteristics on Backwater Rise and Potential for Sediment Transport

The flow distribution equation (Equation 3) in combination with the backwater rise model (Equations 4–6, Follett et al., 2020) was used to explore the backwater rise and associated change in bed shear velocity in the gap, $u_{*,g}$, for a wider range of jam widths than tested in this study. The bed shear velocity was used as a metric for potential sediment transport. First, to explore the impact of jam width and solid volume fraction, we fixed the following

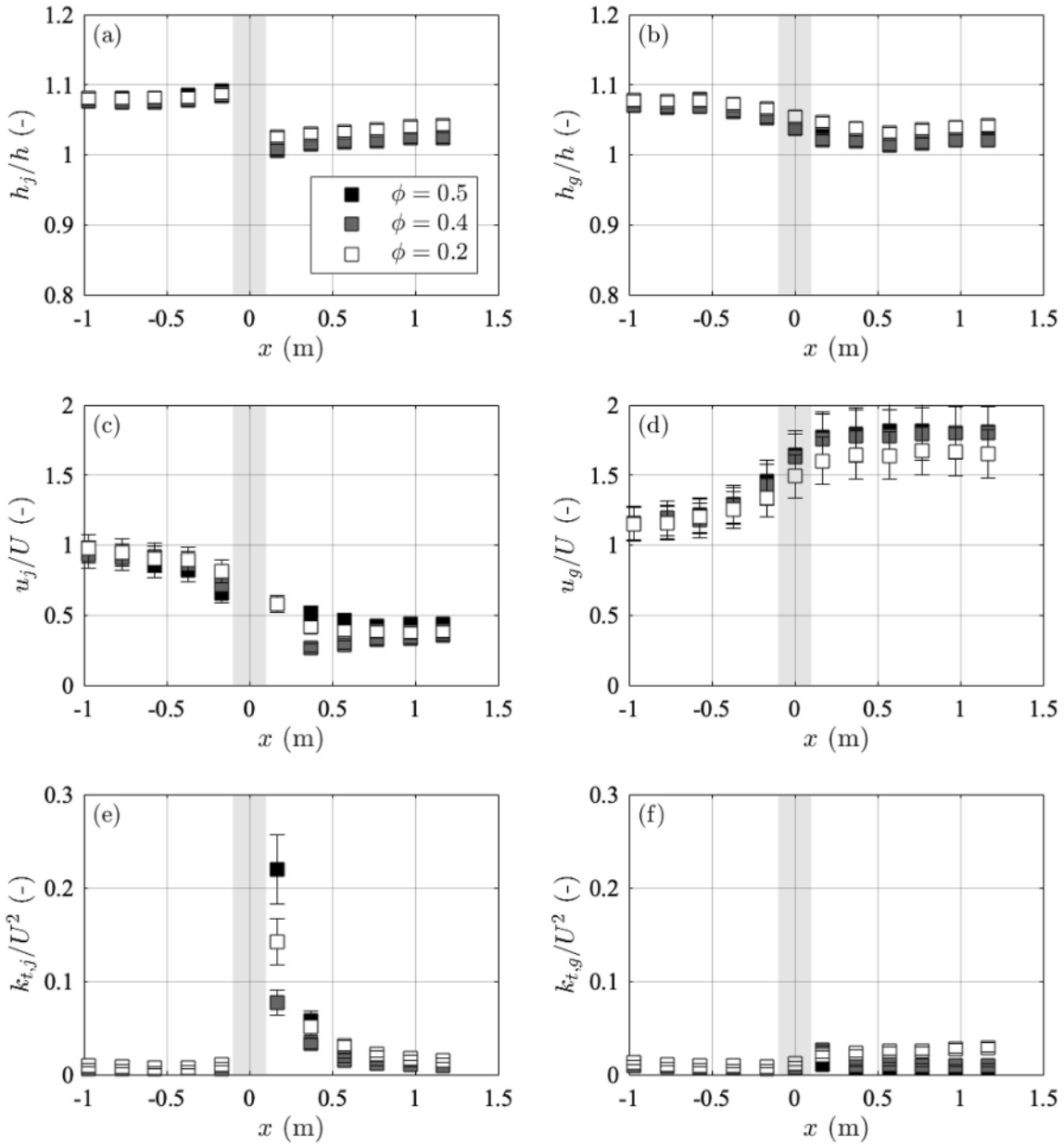

Figure 5. Longitudinal profiles of normalized water depth, time-mean velocity, and turbulent kinetic energy along the jam center (a, c, e) and gap center (b, d, f) for different solid volume fractions $\phi = 0.5$, 0.4, 0.2, and for $B_j = 0.50$ m, $U = 0.30$ m/s (tests 11, 18, 20 in Table 1).

parameters: discharge $Q = 1$ m^3/s, reference water depth $h = 1.1$ m, jam length $L_j = 1.5$ m, and log diameter $d_L = 0.2$ m (Figure 7). The relative backwater rise h_1/h increased with increasing jam width, reaching a maximum backwater rise for the CSJs (Figure 7a). For example, a jam with $\phi = 0.50$ generated a backwater approximately 2 times the reference water depth for CSJs, but only 1.2 times the reference water depth for jams spanning ¼ of the channel width (Figure 7a). Further, a more compact jam (higher ϕ) was associated with higher backwater rise. For example, given a jam spanning half the channel width ($B_j/B = 0.5$), $\phi = 0.2$ resulted in a backwater of approximately 1.1 times the reference water depth, while a $\phi = 0.5$ generated a backwater 1.3 times the reference water depth (Figure 7a). The effect on backwater-rise of varying jam streamwise length L_j (with $\phi = 0.2$) was less pronounced than the influence of jam compaction ϕ (Figure 7a vs. b). Specifically, for CSJs, backwater rise was approximately 1.1 times the reference water depth for $L_j = 1$ m and increased to 1.2 times the reference water depth for $L_j = 2$ m (Figure 7b). For lower ϕ, the impact of streamwise length was negligible (see $\phi = 0.2$ in Figure 7b). Note that the dimensionless structural parameter C_A contains both L_j and ϕ, whereas ϕ has the largest

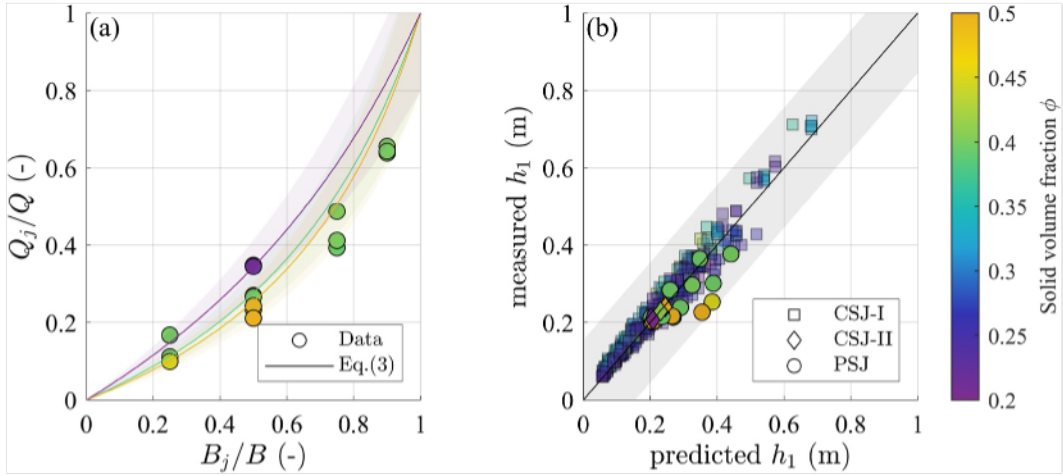

Figure 6. (a) Fraction of discharge through the logjam Q_j/Q versus relative logjam width B_j/B for partial logjams (tests 4–20); (b) predicted (using Equations 4–6) versus measured water depth upstream of the logjam h_1 for partial-spanning jams (PSJ; tests 4–20) and channel-spanning jams (CSJ-I: data from Schalko et al. (2018), CSJ-II: tests 1–3). Prediction of h_1 according to Follett et al. (2020). Line of equality $y = x$ plotted in solid black. The shaded areas correspond to the average relative errors of Equations 3–6.

effect on C_A with an exponent of 3. In addition, C_g may also be a function of jam length, but this was not explored in this study.

The uncertainties associated with the equations used to determine the flow distribution and backwater rise were evaluated with error propagation analyses and reproducibility tests. This is important for application in the field. In contrast to complex logjams in nature, we simplified the jams to consist of only logs without organic fine material such as branches or leaves, which represents a newly formed jam. The range of solid volume fractions tested in this study corresponded to the range of solid volume fractions in the field (Livers et al., 2020). However, the solid volume fraction may not be homogenous across the jam width, which can impact the flow conditions close to the jam, but has less impact after several water depths downstream (Porter, 2022). In addition, the jam shape was constant and model logs were fully rigid. In the field, reconfiguration of flexible elements, such as small branches and leaves, could reduce the jam drag. Specifically, during high flows, backwater rise may be reduced if elements within the jam can reconfigure. To improve predictions of flow distribution and backwater rise in the field, we must develop accurate ways to remotely sense or infer the characteristics of jams (Follett et al., 2020; Livers et al., 2020; Spreitzer et al., 2022). For example, Follett et al. (2020) described how water surface measurements made during a subset of flow conditions could be used to infer the internal logjam drag (C_d a), which subsequently could be used to predict backwater rise at other flow conditions.

Second, as a PSJ leads to flow acceleration in the gap, erosion may occur in the gap section. Figure S10 (Supporting Information S1) shows an example of a CSJ that became partial-spanning due to erosion, with flow distributed through logjam and gap sections. Initiation of erosion may occur if the shear velocity in the gap exceeds the critical threshold, $u_{*,g}/u_{*,cr} > 1$. The critical shear velocity $u_{*,cr}$ was estimated from the critical Shields parameter $\theta_{cr} = 0.047$ (for example, Julien (2010)) with

$$u_{*,cr} = \sqrt{\frac{\theta_{cr} g(\rho_s - \rho) d_m}{\rho}} \tag{8}$$

with $\rho_s = 2{,}650$ kg/m^3. For three particle diameters, $d_{m1} = 6$ mm (fine gravel), $d_{m2} = 20$ mm (medium gravel), and $d_{m3} = 60$ mm (coarse gravel), the critical shear velocity is $u_{*,cr1} = 67.6$ mm/s, $u_{*,cr2} = 123.4$ mm/s, and $u_{*,cr3} = 213.6$ mm/s, respectively.

To assess the likelihood of logjam-generated sediment transport, the critical threshold values were compared to the shear velocity in the gap region:

$$u_{*,g} = \sqrt{C_f} u_g \tag{9}$$

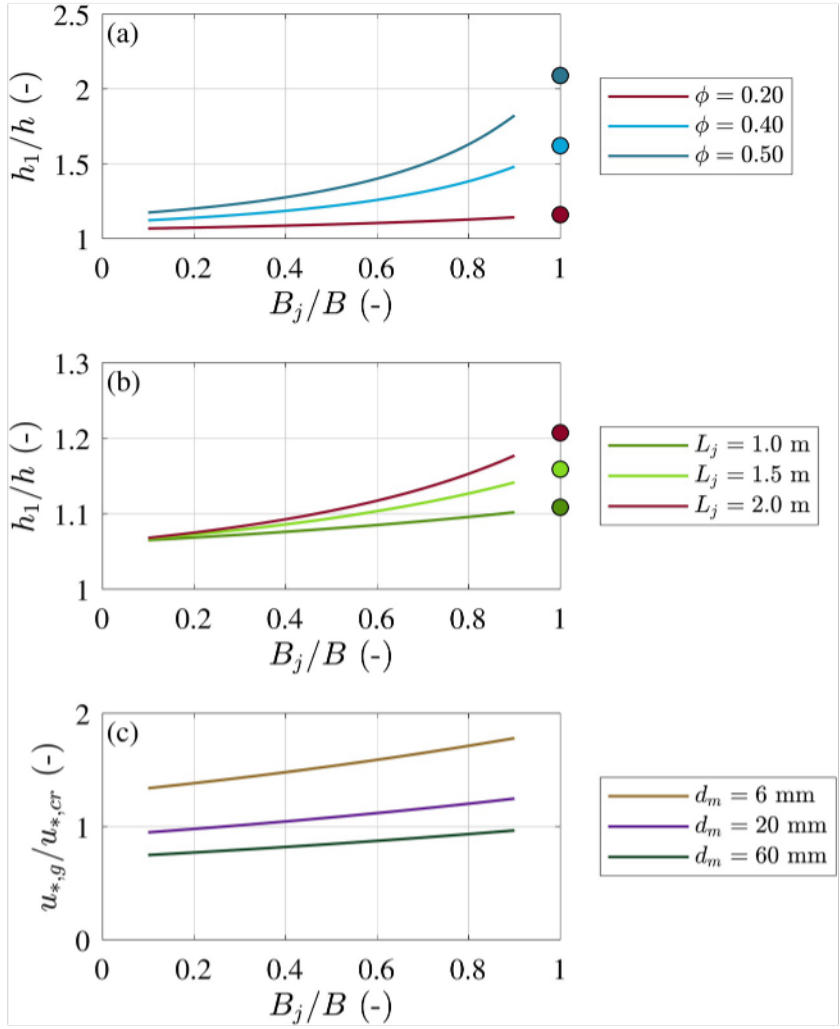

Figure 7. Upstream water depth normalized with reference water depth h_1/h versus relative jam width B_j/B for different (a) solid volume fraction ϕ with $L_j = 1.5$ m and (b) jam lengths L_j with $\phi = 0.2$. (c) Normalized shear velocity in gap with critical shear velocity u_{*g}/u_{*cr} of three different grain sizes $d_m = 6$ mm, 20 mm, and 60 mm versus relative jam width B_j/B. For all cases, discharge $Q = 1$ m^3/s, reference water depth $h = 1.1$ m, and log diameter $d_L = 0.2$ m. Note that the effect of relative jam length was explored without specifying a channel width. In nature, jam length L_j will likely be constrained by channel width. Circles correspond to channel-spanning logjams.

with C_f the bed friction coefficient defined by the semi-empirical equation in Julien (2010):

$$C_f = \frac{1}{\left[5.75 \log\left(\frac{2h}{d_m}\right)\right]^2} \tag{10}$$

with the water depth h defined as h_g = water depth in the gap section. Note that Equation 10 was derived for a uniform-flow log-law profile. Within the gap, accelerating flow can depress the boundary layer, which would enhance C_f, such that Equation 10 represents a lower bound. Future work should investigate determination of C_f for conditions in the gap section.

Across all conditions considered, the measured water depth in the gap h_g ($x = 0$) was a constant fraction of the upstream depth h_1. Specifically, $h_g = 0.74\ h_1$ with 95% confidence interval (0.64, 0.83). The velocity in the gap u_g was determined from the discharge through the gap, $u_g = Q_g/(h_g\ (B–B_j))$, with $Q_g = Q–Q_j$ and Q_j calculated from Equation 3. As expected, the shear velocity in the gap increased with decreasing gap width (i.e., increasing jam width), as the velocity through the gap section increased (Figure 7c), similar to a groyne (Ibrahim, 2014; McCoy

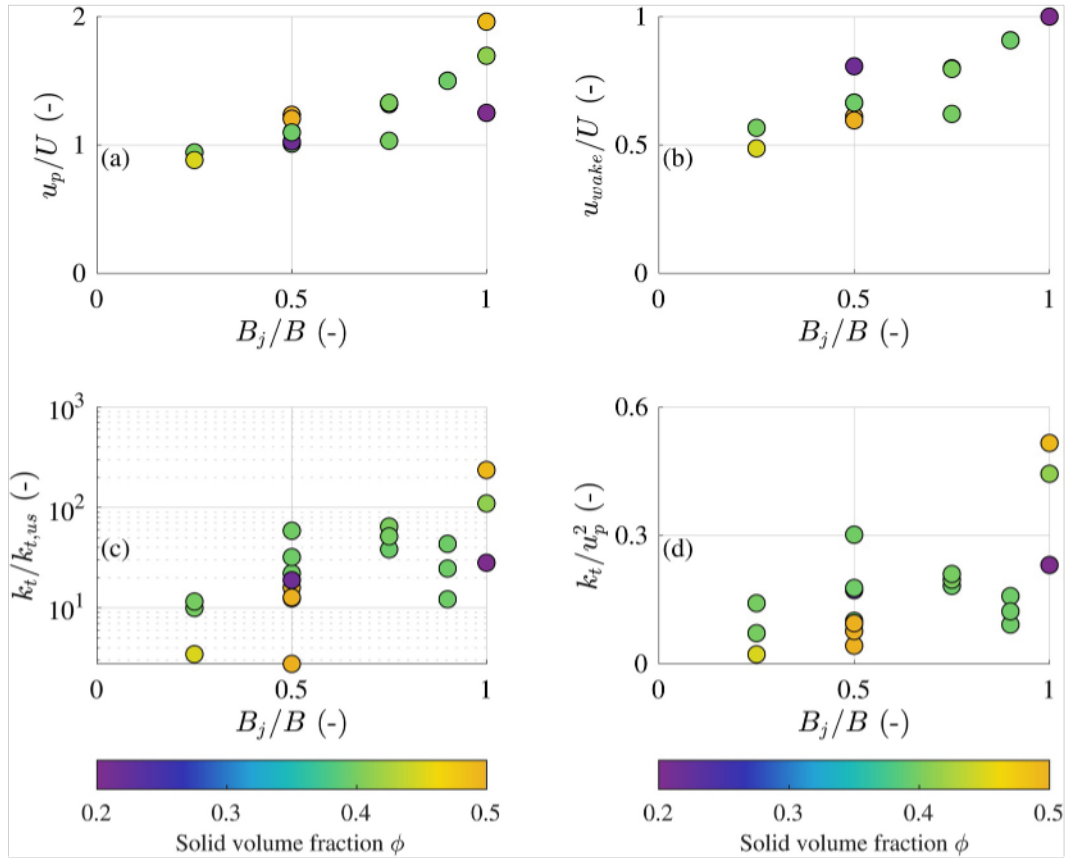

Figure 8. (a) Normalized pore velocity u_p/U, (b) normalized wake velocity u_{wake}/U, (c) normalized TKE $k_t/k_{t,us}$, and (d) normalized TKE k_t/u_p^2 versus relative logjam width B_j/B for different solid volume fraction ϕ.

et al., 2008). Specifically, for $d_m = 20$ mm, $u_{*,g}/u_{*,cr} > 1$ for logjams spanning more than a third of the channel width ($B_j/B > 0.3$). To summarize, both backwater rise and the potential for erosion increase with increasing logjam width. This highlights the relevance to consider flood and geomorphic hazard aspects together when designing jams for river restoration projects.

5.2. Design of Logjams to Improve Flow Heterogeneity

To evaluate the potential to capture fine material and organic matter within the logjam, an important parameter is the average pore velocity u_p in the logjam:

$$u_p = \frac{q_j}{(h_{3,j}(1-\phi))} \tag{11}$$

with the unit discharge through the jam q_j derived using Equation 3, $h_{3,j}$ is the water depth downstream of the jam based on Equation 5, and ϕ is the solid volume fraction. According to the experiments in this study, normalized pore velocity through the jam increased with increasing jam width (Figure 8a). Specifically, u_p was approximately 0.9 times the channel-average reference velocity U for a quarter spanning jam, but increased to approximately 1.7 times U for a CSJ (Figure 8a). Because a higher pore velocity may inhibit deposition of organic matter and particulate nutrients within the jam, wider logjams may be less efficient in trapping these materials, which are needed to enhance habitat. Similarly, the velocity in the wake $u_{wake} = Q_j/(B_j\, h_{3,j})$ increased with increasing jam width (Figure 8b). The minimum u_{wake} corresponded to the smallest jam width $B_j = 0.25$ m, for which u_{wake} was approximately 50% of U. Based on the lateral velocity profile measured downstream of the jam (Figure S4 in Supporting Information S1), the laterally-average u_{wake} was consistently positive, but flow recirculation (negative velocity) was observed to occur locally, due to the heterogeneous composition of logjams.

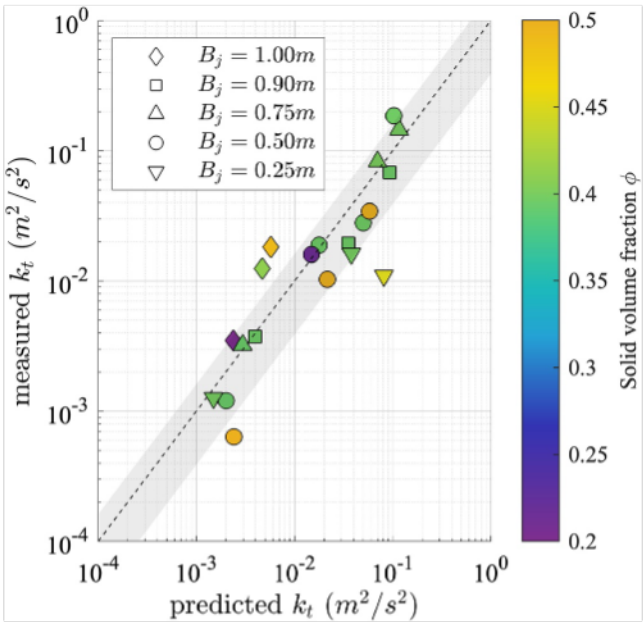

Figure 9. Measured versus predicted turbulent kinetic energy k_t using Equation 12 downstream of the logjam for varying jam widths B_j and solid volume fractions ϕ with line of equality $y = x$ plotted in dashed black. The gray shaded area corresponds to the average relative error associated with Equation 12.

Previous studies have noted that both velocity and turbulence magnitude impact the quality of fish habitat (Golpira et al., 2020; Muhawenimana et al., 2019; Tritico & Cotel, 2010). Based on the observations presented in this study, both velocity and turbulence in the wake decreased with decreasing logjam width (Figure 3). This agrees with findings from experiments on single log placements (Schalko et al., 2021). In contrast, over the tested range of solid volume fraction ($\phi = 0.2$–0.5), ϕ had little impact on the velocities in the wake region (Figure 5). This aligns with findings from studies on vegetation patches (Nicolle & Eames, 2011; Zong & Nepf, 2012) that demonstrated that for $\phi > 0.15$, the wake flow structure of a porous patch resembled that of a solid object, with no dependence on ϕ. As the tested ϕ in this study are all higher than the threshold from literature, no difference in the wake velocity structure was observed in the wake region (Figure 5).

It is important to consider TKE using two normalizations, based on upstream turbulence level (Figure 8c) and on pore velocity (Figure 8d). First, normalizing by the upstream turbulence level emphasizes the elevation of TKE due to the jam. The enhancement of turbulence, relative to upstream $k_t/k_{t,\mathrm{us}}$, increased as jam width increased (Figure 8c). For example, TKE due to a CSJ was elevated in the range of 28–236 compared to the upstream TKE, while a quarter spanning jam only increased TKE by a factor of 3–12. The difference in turbulence level may be linked to different physical habitat preferences of fish species and stages. For example, jams with a relative width of $B_j/B > 0.5$ may establish a downstream flow region preferred by stronger fish species or adult fish due to the stronger turbulence and higher drift densities due to increased velocity next to the logjam. In contrast, jams with $B_j/B < 0.5$ may create flow regions with weaker turbulence, which is preferred by weaker fish species or juvenile fish (Golpira et al., 2020; Liao et al., 2003; Lupandin, 2005; Tullos & Walter, 2015). This emphasizes how similar to the variation of submergence level of groynes (Uijttewaal, 2005) or logs (Schalko et al., 2021), the variation of logjam width may be leveraged to create habitat suitability for different fish preferences.

The second normalization of turbulence by ${u_p}^2$ highlights the generation of turbulence within the logjam. This turbulence is generated at the scale of the log, and decays over length-scales set by the log diameter, similar to grid-generated turbulence, and not the turbulence generated by separation around the logjam. Normalized in this way, the TKE was of a similar order of magnitude for all jam widths in this study, but showed a weak increase with increasing jam width (Figure 8d). For example, for the CSJ, ${k_t/u_p}^2$ spanned 0.23 to 0.52, compared a span of 0.02–0.14 for a quarter spanning jam (Figure 8d). To evaluate the habitat with respect to turbulence, it is useful to have a prediction of turbulence in the vicinity of the jam. We adapted a model for vegetation-generated turbulence developed by Tanino and Nepf (2008). For a dense emergent jam, defined by $d/s \geq 0.56$, the log-generated turbulence can be described by Equation 4.1 in Tanino and Nepf (2008):

$$k_t = {\delta_{kt,l}}^2 \left[C_d \frac{s}{d} \frac{\phi}{(1-\phi)^{\pi/2}} \right]^{2/3} u_p^2 \tag{12}$$

with scaling constant $\delta_{kt,l}$ and jam drag coefficient $C_d = 1.2 \pm 0.6$ according to Figure S1 (Supporting Information S1). We compared this to measured values of TKE averaged across the jam width, using the lateral profiles at the downstream edge of the jam (Figure 9), from which we found the best-fit scale constant $\delta_{kt,l} = 0.70 \pm 0.06$ ($\pm$ standard error; with 95% confidence interval (0.58, 0.82)). This was comparable to $\delta_{kt,v} = 0.88$ observed in an array of parallel cylinders (Tanino & Nepf, 2008), which demonstrated that the TKE generation in the jam, with randomly oriented logs, was similar to that of a more ordered array of parallel structures. The gray shaded area in Figure 9 corresponds to the average relative error of Equation 12 being 62% based on an error propagation analysis (see Table S1 in Supporting Information S1).

Note that the elevated log-scale turbulence only exists within a short distance downstream of the jam. Specifically, TKE decay occurs over ≈60 cm (Figures 3–5), corresponding to ≈20 log diameters d, or ≈50 log spacings

s. The order of magnitude of the decay of log-generated turbulence is comparable to the decay of grid-generated turbulence at $x/M \approx 40$ with M = grid spacing (Mohamed & Larue, 1990). Similar to the placement of individual emergent logs placed at the channel side, a second turbulence peak, associated with the jam width B_j, may occur at $L_{TKE} = (12 \pm 2)\ B_j$ (Schalko et al., 2021). However, this distance was out of the measurement grid of this present study.

Equation 12 can be used in the field to assess the contribution of log-scale turbulence to the jam wake directly downstream from the jam. The surface-to-surface distance between the logs is defined as $s = (d/a)^{1/2}–d$, with d the log diameter and a the spatially-averaged frontal area per jam volume, estimated using $a = (4\ \phi)/(\pi\ d)$. This can be simplified to $s = ((\pi/4\ \phi)^{1/2}–1)\ d$. The log diameter d can be derived from forest inventories. Based on literature, $\phi = 0.2–0.5$ (Livers et al., 2020). If no data are available, a sensitivity analysis of d and ϕ should be performed. The pore velocity u_p can be estimated using Equation 11, which requires information on the unit discharge through the logjam q_j that can be obtained with Equation 3 and water depth downstream of the jam $h_{3,j}$ using Equation 5. This adapted model provides a useful tool to determine log-generated turbulence for varying solid volume fractions to improve the logjam design.

6. Conclusions

The presence of logjams in river systems promotes habitat complexity by increasing heterogeneity of flow and sediment transport. Compared to a channel-spanning logjam, the presence of even a small gap was shown to significantly reduce the backwater rise, but also to increase the erosion risk in the gap. Both backwater rise and velocity in the gap decreased as gap width increased (logjam width decreased). It is important to understand the trade-off between backwater rise and erosion potential to manage existing logjams and to design sustainable logjam restoration.

We showed that the flow distribution can be predicted by assuming that the logjam and gap sections act as parallel resistors, with equal resistance between the logjam and gap sections. Subsequently, the backwater rise can be predicted from the discharge through the logjam, following equations developed for channel-spanning logjams.

The results demonstrated the creation of two distinct flow regions downstream of the logjam cross-section, with reduced velocity in the logjam wake region and elevated velocity downstream of the gap. The distinction between these regions increased with logjam width and may be linked to different habitat preferences of fish species and life stages. Second, the potential for trapping organic matter in the logjam should increase with decreasing pore velocity, which was associated with decreasing logjam width. Third, turbulent kinetic energy was increased directly downstream of the logjam. A prediction of log-generated turbulence provides a new tool for evaluating logjam design.

To conclude, the new predictions for flow distribution, backwater rise, and log-generated turbulence presented in this paper can improve the design and management of engineered logjams used in nature-based solutions as well as the analysis of existing natural logjams. Furthermore, the data set provided may be useful to validate numerical models, which can provide additional detail of the flow structures around natural or engineered logjams.

Conflict of Interest

The authors declare no conflicts of interest relevant to this study.

Data Availability Statement

The data set for this study is available in Schalko (2023) (CC BY 4.0).

Acknowledgments
Antonia Baumann, Nathalie Flury, and Jonathan Rimle are acknowledged for their great laboratory assistance in the frame of their master and project theses at ETH Zurich. The first author is funded by the Swiss National Science Foundation (SNSF) Ambizione Fellowship project No. 209091. The second author has received funding from the Royal Academy of Engineering's Research Fellowships program and the European Regional Development Fund through the Welsh Government Sêr Cymru program 80762-CU-241. We further want to thank three anonymous reviewers for their constructive comments.

References

Abbe, T. B., & Montgomery, D. R. (2003). Patterns and processes of wood debris accumulation in the Queets river basin, Washington. *Geomorphology*, *51*(1), 81–107. https://doi.org/10.1016/s0169-555x(02)00326-4

Beckman, N. D., & Wohl, E. (2014). Carbon storage in mountainous headwater streams: The role of old-growth forest and logjams. *Water Resources Research*, *50*(3), 2376–2393. https://doi.org/10.1002/2013WR014167

Bilby, R. E. (1981). Role of organic debris dams in regulating the export of dissolved and particulate matter from a forested watershed. *Ecology*, *62*(5), 1234–1243. https://doi.org/10.2307/1937288

Brooks, A. P. (2013). Design guideline for the reintroduction of wood into Australian streams (land and water Australia) (p. 85). Retrieved from http://reefcatchments.com.au/files/2013/02/Design-Guideline-for-the-reintroduction-of-wood-into-Australian-streams1.pdf

Bureau of ReclamationU.S. Army Engineer Research and Development Center (USBR & ERDC). (2016). National large wood manual: Assessment, planning, design, and maintenance of large wood in fluvial ecosystems: Restoring process, function, and structure. Retrieved from https://www.usbr.gov/research/projects/download_product.cfm?id=1481

Comiti, F., Lucía, A., & Rickenmann, D. (2016). Large wood recruitment and transport during large floods: A review. *Geomorphology*, *269*, 23–39. https://doi.org/10.1016/j.geomorph.2016.06.016

Davidson, S. L., MacKenzie, L. G., & Eaton, B. C. (2015). Large wood transport and jam formation in a series of flume experiments: Large wood mobilization and transport. *Water Resources Research*, *51*(12), 10065–10077. https://doi.org/10.1002/2015WR017446

Doughty, M., Sawyer, A. H., Wohl, E., & Singha, K. (2020). Mapping increases in hyporheic exchange from channel-spanning logjams. *Journal of Hydrology*, *587*, 124931. https://doi.org/10.1016/j.jhydrol.2020.124931

Faustini, J. M., & Jones, J. A. (2003). Influence of large woody debris on channel morphology and dynamics in steep, boulder-rich mountain streams, western Cascades, Oregon. *Geomorphology*, *51*(1–3), 187–205. https://doi.org/10.1016/S0169-555X(02)00336-7

Follett, E., Schalko, I., & Nepf, H. (2020). Momentum and energy predict the backwater rise generated by a large wood jam. *Geophysical Research Letters*, *47*(17), e2020GL089346. https://doi.org/10.1029/2020GL089346

Follett, E., Schalko, I., & Nepf, H. (2021). Logjams with a lower gap: Backwater rise and flow distribution beneath and through logjam predicted by two-box momentum balance. *Geophysical Research Letters*, *48*(16), e2021GL094279. https://doi.org/10.1029/2021GL094279

Gippel, C. J. (1995). Environmental hydraulics of large woody debris in streams and rivers. *Journal of Environmental Engineering*, *121*(5), 388–395. https://doi.org/10.1061/(ASCE)0733-9372(1995)121:5(388)

Golpira, A., Baki, A. B., & Zhu, D. Z. (2020). Higher-order velocity moments, turbulence scales and energy dissipation rate around a boulder in a rock-ramp fish passage. *Sustainability*, *12*(13), 5385. https://doi.org/10.3390/su12135385

Goring, D. G., & Nikora, V. I. (2002). Despiking acoustic Doppler velocimeter data. *Journal of Hydraulic Engineering*, *128*(1), 117–126. https://doi.org/10.1061/(ASCE)0733-9429(2002)128:1(117)

Gurnell, A. M., PiéGay, H., Swanson, F. J., & Gregory, S. V. (2002). Large wood and fluvial processes: Large wood and fluvial processes. *Freshwater Biology*, *47*(4), 601–619. https://doi.org/10.1046/j.1365-2427.2002.00916.x

Ibrahim, M. M. (2014). Local bed morphological changes due to oriented groins in straight channels. *Ain Shams Engineering Journal*, *5*(2), 333–341. https://doi.org/10.1016/j.asej.2013.12.006

Julien, P. Y. (2010). *Erosion and sedimentation* (2nd ed.). Cambridge University Press.

Keller, E. A., & Swanson, F. J. (1979). Effects of large organic material on channel form and fluvial processes. *Earth Surface Processes*, *4*(4), 361–380. https://doi.org/10.1002/esp.3290040406

Liao, J. C., Beal, D. N., Lauder, G. V., & Triantafyllou, M. S. (2003). The Karman gait: Novel body kinematics of rainbow trout swimming in a vortex street. *Journal of Experimental Biology*, *206*(6), 1059–1073. https://doi.org/10.1242/jeb.00209

Livers, B., Lininger, K. B., Kramer, N., & Sendrowski, A. (2020). Porosity problems: Comparing and reviewing methods for estimating porosity and volume of wood jams in the field. *Earth Surface Processes and Landforms*, *45*(13), 3336–3353. https://doi.org/10.1002/esp.4969

Livers, B., & Wohl, E. (2021). All logjams are not created equal. *Journal of Geophysical Research: Earth Surface*, *126*(8), e2021JF006076. https://doi.org/10.1029/2021JF006076

Lucía, A., Comiti, F., Borga, M., Cavalli, M., & Marchi, L. (2015). Dynamics of large wood during a flash flood in two mountain catchments. *Natural Hazards and Earth System Sciences Discussions*, *3*(2), 1643–1680. https://doi.org/10.5194/nhessd-3-1643-2015

Lupandin, A. I. (2005). Effect of flow turbulence on swimming speed of fish. *Biology Bulletin*, *32*(5), 461–466. https://doi.org/10.1007/s10525-005-0125-z

Manners, R. B., & Doyle, M. W. (2008). A mechanistic model of woody debris jam evolution and its application to wood-based restoration and management. *River Research and Applications*, *24*(8), 1104–1123. https://doi.org/10.1002/rra.1108

Martin, H., & Pohl, R. (2015). *Technische Hydromechanik 4 (Technical hydromechanics 4)*. Verlag Bauwesen.

McCoy, A., Constantinescu, G., & Weber, L. J. (2008). Numerical investigation of flow hydrodynamics in a channel with a series of groynes. *Journal of Hydraulic Engineering*, *134*(2), 157–172. https://doi.org/10.1061/(asce)0733-9429(2008)134:2(157)

Mohamed, M. S., & Larue, J. C. (1990). The decay power law in grid-generated turbulence. *Journal of Fluid Mechanics*, *219*(1), 195. https://doi.org/10.1017/S0022112090002919

Muhawenimana, V., Wilson, C. A. M. E., Ouro, P., & Cable, J. (2019). Spanwise cylinder wake hydrodynamics and fish behavior. *Water Resources Research*, *55*(11), 8569–8582. https://doi.org/10.1029/2018WR024217

Nakamura, F., & Swanson, F. J. (1994). Distribution of coarse woody debris in a mountain stream, western Cascade Range, Oregon. *Canadian Journal of Forest Research*, *24*(12), 2395–2403. https://doi.org/10.1139/x94-309

Neuhaus, V., & Mende, M. (2021). Engineered large wood structures in stream restoration projects in Switzerland: Practice-based experiences. *Water*, *13*(18), 2520. https://doi.org/10.3390/w13182520

Nicolle, A., & Eames, I. (2011). Numerical study of flow through and around a circular array of cylinders. *Journal of Fluid Mechanics*, *679*, 1–31. https://doi.org/10.1017/jfm.2011.77

Pagliara, S., & Kurdistani, S. M. (2017). Flume experiments on scour downstream of wood stream restoration structures. *Geomorphology*, *279*, 141–149. https://doi.org/10.1016/j.geomorph.2016.10.013

Piégay, H., Gregory, K. J., Bondarev, V., Chin, A., Dahlstrom, N., Elosegi, A., et al. (2005). Public perception as a barrier to introducing wood in rivers for restoration purposes. *Environmental Management*, *36*(5), 665–674. https://doi.org/10.1007/s00267-004-0092-z

Pope, S. B. (2000). *Turbulent flows*. Cambridge University Press.

Porter, R. C. (2022). Wake characteristics associated with logjams to inform river restoration. (Master Thesis). Massachusetts Institute of Technology. Retrieved from https://hdl.handle.net/1721.1/144585

Roni, P., Beechie, T., Pess, G., & Hanson, K. (2015). Wood placement in river restoration: Fact, fiction, and future direction. *Canadian Journal of Fisheries and Aquatic Sciences*, *72*(3), 466–478. https://doi.org/10.1139/cjfas-2014-0344

Sawyer, A. H., Bayani Cardenas, M., & Buttles, J. (2011). Hyporheic exchange due to channel-spanning logs. *Water Resources Research*, *47*(8), W08502. https://doi.org/10.1029/2011WR010484

Schalko, I. (2023). Dataset: Impact of lateral gap on flow distribution, backwater rise, and turbulence generated by a logjam [Dataset]. Zenodo. https://doi.org/10.5281/ZENODO.8415089

Schalko, I., Lageder, C., Schmocker, L., Weitbrecht, V., & Boes, R. M. (2019a). *Laboratory flume experiments on the formation of spanwise large wood accumulations Part I: Effect on backwater rise*. Water Resources Research.

Schalko, I., Lageder, C., Schmocker, L., Weitbrecht, V., & Boes, R. M. (2019b). *Laboratory flume experiments on the formation of spanwise large wood accumulations Part II: Effect on local scour*. Water Resources Research.

Schalko, I., Schmocker, L., Weitbrecht, V., & Boes, R. M. (2018). Backwater rise due to large wood accumulations. *Journal of Hydraulic Engineering*, *144*(9), 04018056. https://doi.org/10.1061/(ASCE)HY.1943-7900.0001501

Schalko, I., Wohl, E., & Nepf, H. M. (2021). Flow and wake characteristics associated with large wood to inform river restoration. *Scientific Reports*, *11*(1), 8644. https://doi.org/10.1038/s41598-021-87892-7

Schmocker, L., & Weitbrecht, V. (2013). Driftwood: Risk analysis and engineering measures. *Journal of Hydraulic Engineering*, *139*(7), 683–695. https://doi.org/10.1061/(ASCE)HY.1943-7900.0000728

Shields, F. D., & Alonso, C. V. (2012). Assessment of flow forces on large wood in rivers: Lift and drag on large wood. *Water Resources Research*, *48*(4), W04516. https://doi.org/10.1029/2011WR011547

Skalak, K., & Pizzuto, J. (2010). The distribution and residence time of suspended sediment stored within the channel margins of a gravel-bed bedrock river. *Earth Surface Processes and Landforms*. https://doi.org/10.1002/esp.1926

Spreitzer, G., Schalko, I., Boes, R. M., & Weitbrecht, V. (2022). Towards a non-intrusive method employing digital twin models for the assessment of complex large wood accumulations in fluvial environments. *Journal of Hydrology*, *614*, 128505. And here is the link to the article. https://doi.org/10.1016/j.jhydrol.2022.128505

Tanino, Y., & Nepf, H. M. (2008). Lateral dispersion in random cylinder arrays at high Reynolds number. *Journal of Fluid Mechanics*, *600*, 339–371. https://doi.org/10.1017/S0022112008000505

Tritico, H. M., & Cotel, A. J. (2010). The effects of turbulent eddies on the stability and critical swimming speed of creek chub (Semotilus atromaculatus). *Journal of Experimental Biology*, *213*(13), 2284–2293. https://doi.org/10.1242/jeb.041806

Tullos, D., & Walter, C. (2015). Fish use of turbulence around wood in winter: Physical experiments on hydraulic variability and habitat selection by juvenile Coho salmon, Oncorhynchus kisutch. *Environmental Biology of Fishes*, *98*(5), 1339–1353. https://doi.org/10.1007/s10641-014-0362-4

Uijttewaal, W. S. (2005). Effects of Groyne layout on the flow in Groyne fields: Laboratory experiments. *Journal of Hydraulic Engineering*, *131*(9), 782–791. https://doi.org/10.1061/(ASCE)0733-9429(2005)131:9(782)

Wallerstein, N., Thorne, C. R., & Abt, S. (1996). *Debris control at hydraulic structures, contract modification: Management of woody debris in natural channels and at hydraulic structures (No. WK2Q6C-8096-EN09)*. US Army Corps of Engineers.

Weitbrecht, V., Socolofsky, S. A., & Jirka, G. H. (2008). Experiments on mass exchange between groin fields and main stream in rivers. *Journal of Hydraulic Engineering*, *134*(2), 173–183. https://doi.org/10.1061/(asce)0733-9429(2008)134:2(173)

Wohl, E., Bledsoe, B. P., Fausch, K. D., Kramer, N., Bestgen, K. R., & Gooseff, M. N. (2016). Management of large wood in streams: An overview and proposed framework for hazard evaluation. *JAWRA*, *52*(2), 315–335. https://doi.org/10.1111/1752-1688.12388

Wohl, E., Kramer, N., Ruiz-Villanueva, V., Scott, D. N., Comiti, F., Gurnell, A. M., et al. (2019). The natural wood regime in rivers. *BioScience*, *69*(4), 259–273. https://doi.org/10.1093/biosci/biz013

Zhang, N., Rutherfurd, I., & Ghisalberti, M. (2020a). Effect of instream logs on bank erosion potential: A flume study with a single log. *Journal of Ecohydraulics*, *5*(1), 43–56. https://doi.org/10.1080/24705357.2019.1634499

Zhang, N., & Rutherfurd, I. D. (2020). The effect of instream logs on river-bank erosion: Field measurements of hydraulics and erosion rates. *Earth Surface Processes and Landforms*, *45*(7), 1677–1690. https://doi.org/10.1002/esp.4838

Zhang, N., Rutherfurd, I. D., & Ghisalberti, M. (2020b). The effect of instream logs on bank erosion potential: A flume study with multiple logs. *Journal of Ecohydraulics*, *5*(1), 57–70. https://doi.org/10.1080/24705357.2019.1669495

Zong, L., & Nepf, H. (2012). Vortex development behind a finite porous obstruction in a channel. *Journal of Fluid Mechanics*, *691*, 368–391. https://doi.org/10.1017/jfm.2011.479